DOI: 10.6060/mhc256989c

Composite Film Materials Based on Cu(II) 5,15-Di(4-aminophenyl)-10,20-diphenylporphyrin and Aniline: Synthesis and Application

Svetlana A. Chulovskaya,[@] Sergey M. Kuzmin, and Vladimir I. Parfenyuk

G.A. Krestov Institute of Solution Chemistry of RAS, 153045, Ivanovo, Russia
Corresponding author: E-mail: chulovskaya@yandex.ru

In the present work, we compared the formation processes and properties of films of Cu(II) 5,15-di(4-aminophenyl)-10,20-diphenylporphyrin (Porph) and a composite (Porph + aniline). The polyporphyrin films were prepared by superoxide-initiated electrochemical deposition. Composite was formed from mixtures of components having the same chemical nature of the electroactive group due to the difference of potential regions during their deposition. The redox potentials of Porph and aniline in dimethyl sulfoxide solutions were determined. The presence of aniline changes the morphology and functional characteristics of composite. It is shown that the reaction of electrochemical reduction of carbon dioxide on the surface of the composite film proceeds more efficiently than on the surface of the poly-Porph film. We believe that this is due to the increased density of surface defects for composite film.

Keywords: Porphyrins, films, deposition kinetics, composite, superoxide-assisted electrochemical deposition method, surface microstructure, carbon dioxide electroreduction.

Пленочные материалы на основе Cu(II) 5,15-ди(4-аминофенил)-10,20-дифенилпорфирина и анилина: синтез и применение

С. А. Чуловская, С. М. Кузьмин, В. И. Парфенюк

Институт химии растворов им. Г. А. Крестова РАН, 153045 Иваново, Россия
[@]E-mail: chulovskaya@yandex.ru

В настоящей работе сопоставлены процессы формирования и свойств пленок Cu(II) 5,15-ди(4-аминофенил)-10,20-дифенилпорфирина и композитного материала (порфирин + анилин). Полипорфириновые пленки получены методом электрохимического осаждения, инициированного супероксидом. Композит формируется из смесей компонентов, имеющих одинаковую химическую природу электроактивной группы, благодаря различию областей потенциалов при их осаждении. Определены потенциалы окислительно-восстановительных процессов компонентов композита в растворах диметилсульфоксида. Присутствие анилина меняет морфологию и функциональные характеристики композита. Показано, что реакция электрохимического восстановления углекислого газа на поверхности композита протекает эффективнее, чем на поверхности полипорфириновой пленки. Мы полагаем, что это обусловлено повышением плотности поверхностных дефектов для пленки композита.

Ключевые слова: Порфирины, пленки, кинетика осаждения, композит, метод электрохимического осаждения с участием супероксида, микроструктура поверхности, электровосстановление диоксида углерода.

Introduction

The specific properties of the tetrapyrrole macrocycle and its architectural flexibility combined with currently available synthetic methodologies make porphyrin derivatives an important object of scientific research.[1] To solve a range of practical problems the porphyrin structure can be modified via introducing various peripheral functional groups as well as metal atoms into the porphyrin core.[2-7] The ability of many porphyrin derivatives to form polymer films has opened up great prospects for their use, which have received various practical applications.[8-10] The search for effective catalysts for the carbon dioxide reduction reaction (CO_2ERR) is a promising area of research for porphyrin materials.[11,12] Firstly, this is due to an increase in the concentration of CO_2 in the atmosphere due to technological emissions and the associated danger of global warming. Secondly, CO_2 recovery allows not only to reduce environmental risks, but also to establish the production of chemicals and fuels using renewable energy sources.[13-15] Metalloporphyrins are considered as an attractive platform for creating CO_2ERR catalysts,[16,17] and porphyrin copper complex catalysts show high efficacy.[18-23]

We have previously shown that substituted tetraphenylporphyrins can electrochemically form a film on the electrode surface from solutions in dimethyl sulfoxide (DMSO) when the process is initiated by superoxide anion radical.[24] The obtained materials were found to possess semiconducting, photovoltaic, and electrocatalytic properties.[25-27] Moreover, for copper complexes of aminophenylporphyrins, the formation of films is possible with the "on" or "off" mechanism of superoxide-initiated polymerization.[25] The potential of porphyrins can also be realized as part of hybrid and composite materials. The merging of the peculiar features single components into hybrid nanostructures results in novel materials with amplified properties exploitable in different application fields.[28-31] Polyaniline is a promising material that exhibits high conductivity and good reversible redox activity. In particular, polyaniline transports free radicals, so it can be used as a catalyst. Composite materials modified with aniline are active in CO_2ERR.[32,33]

The film composite based on Mn(III) 5,10,15,20-tetrakis(4-aminophenyl)porphyrin and aniline showed greater efficiency of the oxygen electroconduction reaction than a film material based on individual porphyrin.[34]

Therefore, consideration of the possibility of forming composite materials containing both metalloporphyrin and aniline, as well as analyzing the activity of these materials in CO_2 ERR is relevant. In this work, the processes of formation of Cu(II) 5,15-di(4-aminophenyl)-10,20-diphenylporphyrin (Porph), aniline and composite material (Porph + aniline) films initiated by superoxide are considered for the first time. The significant effect of the presence of aniline in solution is shown both on the kinetics of the film formation and on the morphology of the surface of the resulting materials. The possibility of using the obtained films as CO_2ERR catalysts is considered. It was found that for the composite in acetonitrile, a lower value of the CO_2ERR start potential and a significant increase in current density are observed compared to the process on the polyporphyrin film. This indicates the possibility of forming catalyst systems with good characteristics.

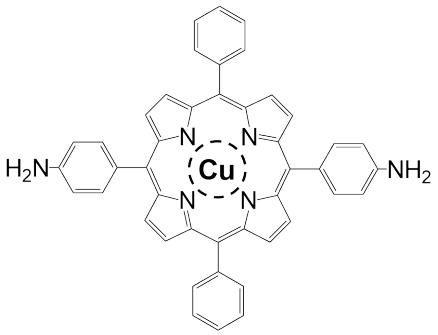

Figure 1. Structure of Cu(II) 5,15-di(4-aminophenyl)-10,20-diphenylporphyrin.

Experimental

Cu(II) 5,15-di(4-aminophenyl)-10,20-diphenylporphyrin was synthesized according to[31], the copper complex was obtained by a well-known technique.[36] The porphyrin structure is shown in Figure 1.

Formation of Porph and composite films was accomplished by superoxide anion radical-initiated electrodeposition from solutions in dimethyl sulfoxide (DMSO).[37]

The deposition of poly-Porph and composite on glassy carbon and indium tin oxide (ITO) from oxygenated DMSO solutions was carried out in a three-electrode electrochemical cell. $Hg/Hg_2Cl_2,Cl^-$ (1 M LiCl) was used as a reference electrode and platinum wire was used as an auxiliary electrode. The films were formed from 10^{-3} M Porph and 10^{-3} M Porph + 10^{-3} M aniline solution for 10 cycles at a potential sweep rate of 0.02 V/sec. 0.02 M tetrabutylammonium perchlorate (TBAP) was used as a background electrolyte. The experiments were performed on a SP-150 potentiostat (Bio-Logic Science Instruments, France) with a QCM922A electrochemical quartz microbalance attachment (SEIKO EG & G, Japan).

The surface morphology of the film materials was studied by atomic force microscopy (AFM) on a Solver-47-Pro microscope (NT-MDT, Russia). The images were processed using Nova RC 1.0.26.1340 software. CO_2RR studies were performed in 0.1 M acetonitrile solutions with 0.02 M TBAP background electrolyte. The solution was first deaerated with argon, and then saturated with bottled carbon dioxide by passing gases for 30 minutes through a bubbling tube.

Linear voltammograms (LSV) were recorded between 0.0 and –2.0 V. The potential sweep rate was 0.01 V/s. The current density was determined using the geometric surface area of the working electrode.

Results and Discussion

The study by quartz microbalance method showed that during the formation of poly-Porph films in the potentiodynamic mode (Figure 2a), the mass gain is observed in the region of oxygen electroreduction. The desorption of the film material coincides with the region of porphyrin electrooxidation potentials (+1.1 to +1.5 V). The intensity of the deposition and desorption waves increases from cycle to cycle (Figure 2a,c). Similar behavior was observed for the formation of polymeric films of aminophenylporphyrins,[37,38] suggesting a superoxide-initiated polymerization mechanism.

The mass gain of polyaniline per cycle is very small (Figure 2c, curve 2). As the number of cycles increases, the desorption waves increase, which does not allow obtaining a film suitable for the study. Despite this, the formation of composite from solutions has a number of characteristic features not observed in the formation of the films of individual constituents.

During the formation of composite films, the mass increase is observed in the region of electroreduction of the solution components and is shifted to more negative potentials (Figure 2b). The film desorption in the electrooxidation region starts at potentials around +0.6 V and is followed by the film mass growth at potentials around +1.3 V. Gradually, two desorption regions (from –1.6 to –2.0 V and from +0.6 to +1.3 V) are formed during composite film deposition. This leads to a more complex dependence Δm(t) in the case of composite film deposition (Figure 2c, curve 3), compared to poly-Porph deposition (Figure 2c, curve 1). Ten potential cycles between –2.0 and +1.5 V lead to mass values of about 4.5 μg for poly-Porph, 0.5 μg for polyaniline and 5.9 μg for composite.

When forming the films based on aminophenylporphyrins, phenazine-like bridges of various types are the most likely type of binding of the porphyrins into a polymer chain (Figure 3).[39,40] Aniline has a different type of binding,[41] which does not contribute to the formation of the copolymer. In addition, precipitation of aminophenylporphyrin and aniline in DMSO occurs at different potentials, so the most likely structure of the composite material may be the formation of the polyporphyrin grains with polyaniline layers between them.

Topographic images of the surface of both films (Figure 4a,b) allow us to observe the differences in the morphology of poly-Porph and composite films. When scanning surface areas of size 10×10 μm, the average roughness (S_a) was 42.1 and 51.2 nm for poly-Porph and composite, respectively. Filamentous formations were observed on the surface of poly-Porph and composite. In the poly-Porph structure, the filaments simply "lie" on the surface. In the composite structure, they are on the boundaries of depressions. The depressions have a transverse size of 1.5–2.5 μm and form a quasi-ordered structure. When scanning a surface area of 1.5×1.5 μm (Figure 4b,c), globules can be observed, which form both relatively flat surface areas and filaments. The lateral size of the globules forming the poly-Porph surface is larger than that of the globules forming the surface of composite film. For poly-Porph, this size ranges from 50 to 200 nm, while for composite it ranges from 30 to 70 nm. The boundaries of the globules can be considered as surface defects, the presence of which enhances the catalytic activity.[37,38,42,43]

The thickness of the resulting films was determined using AFM method. To do this, a part of the film surface was removed from the substrate using a micro-cutter. As can be seen from Figure 5, the resulting profile has the step, the height of which corresponds to the thickness of the film. The totality of measurements performed on different parts of the film shows that the film thickness varies slightly from point to point and is 280 nm for poly-Porph and 310 nm for the composite.

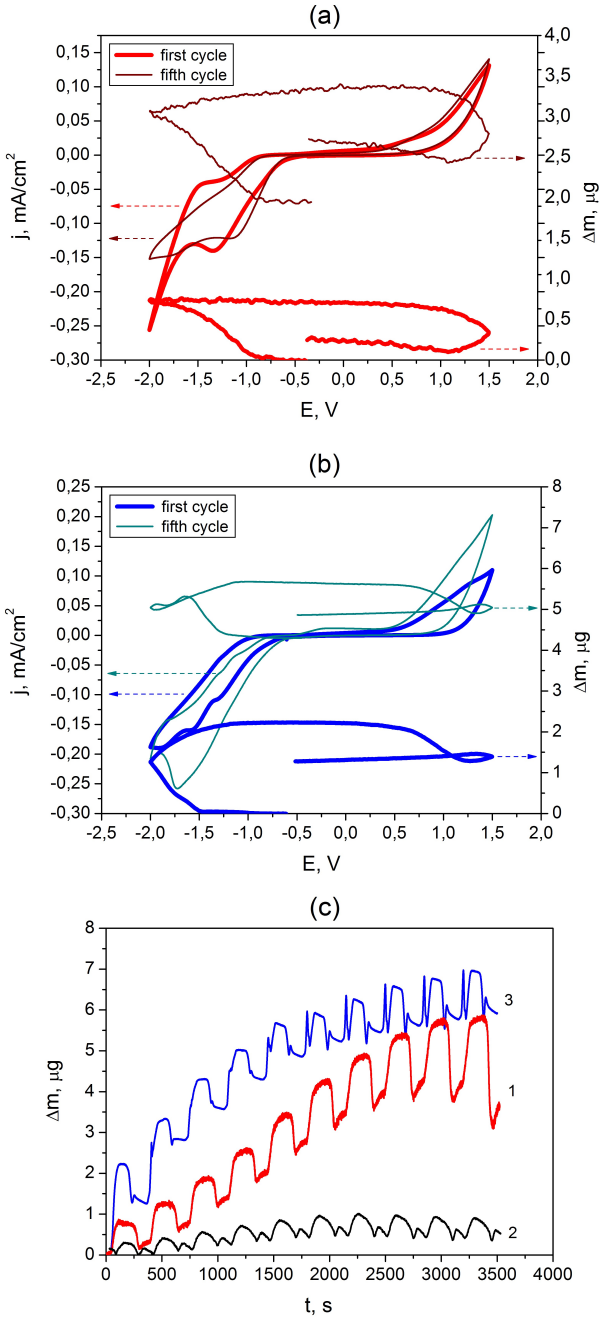

Figure 2. Comparison of cyclic voltammograms and mass change during poly-Porph (a) and composite (b) formation from oxygenated DMSO solutions. The first and fifth cycles are presented. The potential cycling rate is 0.02 V/s. Time dependences of mass (c) during the formation of poly-Porph (curve 1), polyaniline (curve 2) and composite (curve 3).

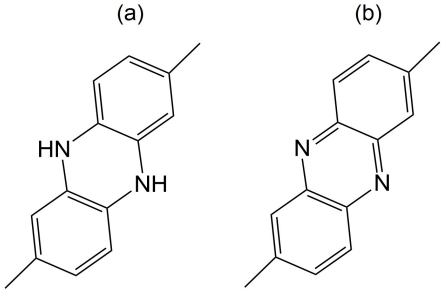

Figure 3. Main types of porphyrin-porphyrin coupling in polymeric aminophenyl: dihydrophenazine (a); phenazine (b).

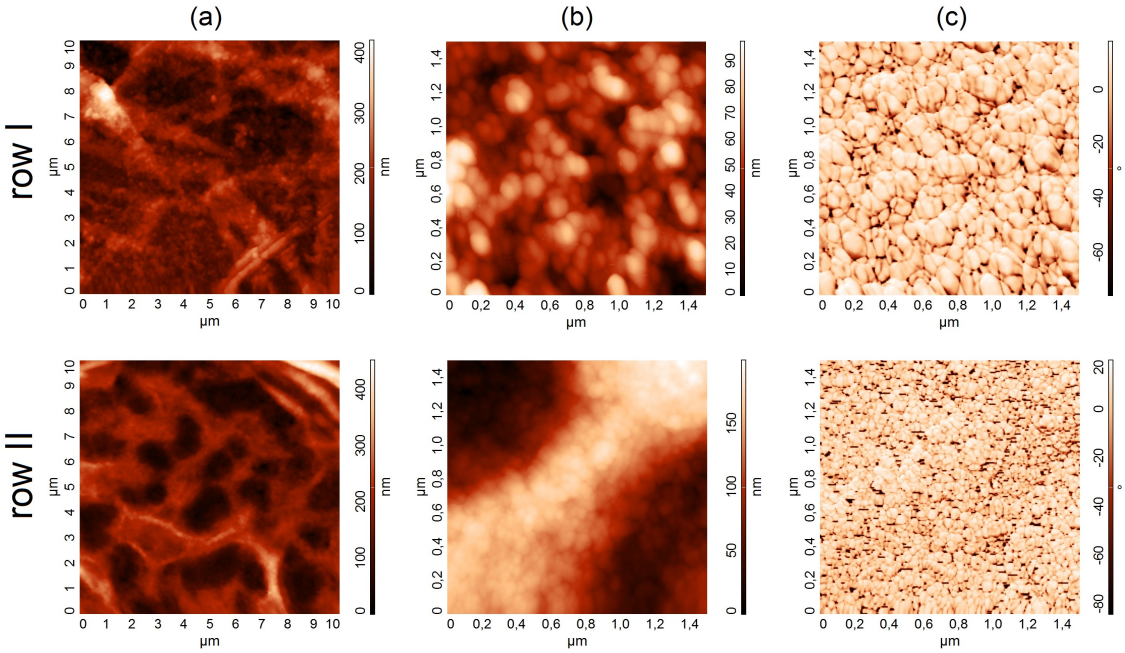

Figure 4. AFM images of the surface of poly-Porph (row I) and composite (row II) films. Topological images (a, b), phase contrast images (c). Scan field: 10x10 µm (a), 1.5x1.5 µm (b, c)

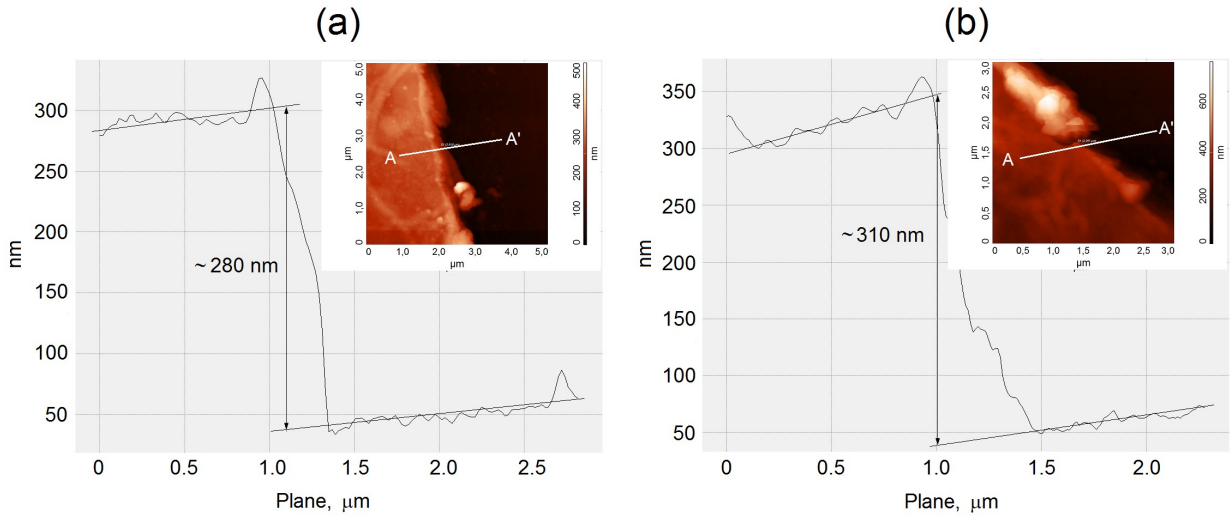

Figure 5. Results of processing AFM images of the formed boundary between the film deposited on the substrate and the pure substrate. Height profile of the step formed by the micro-cutter along the line A-A' (insert) for: a) poly-Porph; b) composite.

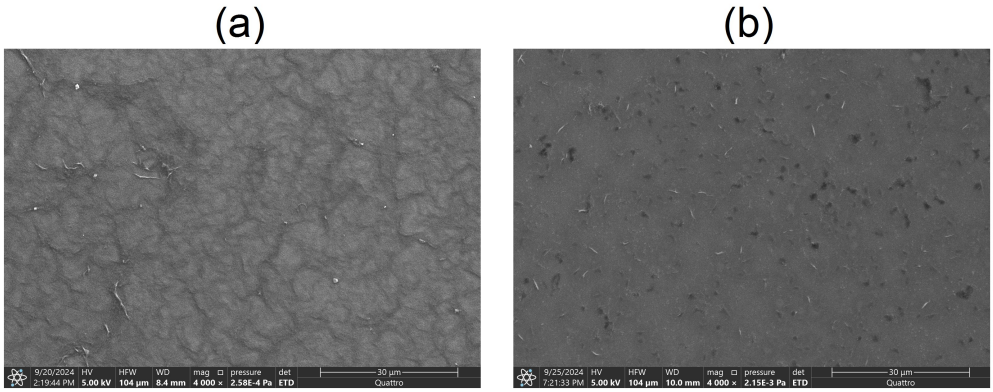

Figure 6. SEM images of poly-Porph (a) and composite (b) surface. Scanning field 30 µm.

Electron micrographs of poly-Porph and composite (Figure 6a,b) demonstrate the difference in the surface structure of these films. Considering that in the SEM method the image is formed by the interaction of electrons with the surface, we can attribute the dark regions of the image to regions with higher conductivity, and the light regions to regions with lower conductivity. For poly-Porph (Figure 6a), the surface contains dark filamentary structures. In addition, light-colored filaments and globules are present on the surface. Short light filaments and localized dark phenocrysts are present on the composite surface (Figure 6b).

Considering the prospects that copper based materials have in the field of CO_2ERR catalysis,[18,19,44,45] we obtained and tested the responses of poly-Porph and composite films prepared on glassy carbon in this process.

The electroreduction of oxygen in oxygenated DMSO proceeds by a one-electron mechanism[46] with the formation of superoxide ($O_2 + e \rightarrow O_2^{\bullet-}$), which is reduced to oxygen ($O_2^{\bullet-} \rightarrow O_2 + e$) (Figure 7a). The electrochemical responses of Porph in degassed DMSO solution (Figure 7b, curve 1) demonstrate the presence of the porphyrin reduction and oxidation processes. Two electroreduction processes are observed with current peak potentials around –1.25 V and –1.75 V. The pair of peaks –1.25/–1.17 V is most likely related to the change in the charge of the metal center. The oxidation of Porph is irreversible and is explained by intramolecular transfer of excess electrons to the porphyrin ring with the formation of π-cation radicals. The shape of CV curves does not change upon cycling. The polyporphyrin film on the surface of the working electrode after tenfold cycling of the potential was not observed. For Porph in oxygenated DMSO solutions (Figure 7c, curve 2), the CV shape changes from cycle to cycle. The ratio of cathodic current peak to anodic current peak decreases with cycling. These changes in the electrochemical response of the $O_2^{\bullet-}$ radical are attributed to its interaction with the monomeric form of the porphyrin and with the forming film. After tenfold potential cycling, a yellowish-brown colored polyporphyrin film was observed on the surface of the working electrode.

The electrochemical response in degassed DMSO solution (Figure 7c, curve 1) demonstrates the presence of aniline oxidation process at a potential of about +1.10 V. The oxidation is irreversible. No polyaniline film on the surface of the working electrode was observed after cycling the potential ten times. For composite in oxygenated DMSO solutions (Figure 7b, curve 2), the CV shape changes from cycle to cycle. The ratio of cathodic current peak to anodic current peak decreases with cycling. In the region around 0.0 V, a peak appears corresponding to the electroreduction of the oxidized amino group of aniline, which was not observed during the formation of the poly-Porph film. After tenfold potential cycling, a yellowish-brown polyporphyrin film was observed on the surface of the working electrode. Thus, the addition of aniline changes both the structure of films (Figures 4–6) and RedOx behavior during film formation (Figure 7).

LSV of carbon dioxide electroreduction (Figure 8) showed a shift of the onset on the composite surface to the positive region compared to the onset on glassy carbon and poly-Porph. A current density of 0.05 mA/cm^2 for CO_2ERR is achieved on glassy carbon at a potential of –1.15 V, at a potential of –1.02 V for poly-Porph, and at a potential of –0.72 V for composite. The shift in the onset potential of CO_2ERR and the increase in current evidence high composite activity in this process. The LSV of CO_2ERR contains a region of sharp increase in current density at a potential of approximately –0.88 V and maxima at potentials of –1.14 V, –1.45 V, and –1.72 V. This behavior indicates the multi-stage nature of CO_2ERR. The offset potential and current density of CO_2ERR obtained in this work are not inferior to the results obtained under similar conditions for catalysts of various types under similar conditions.[22,47]

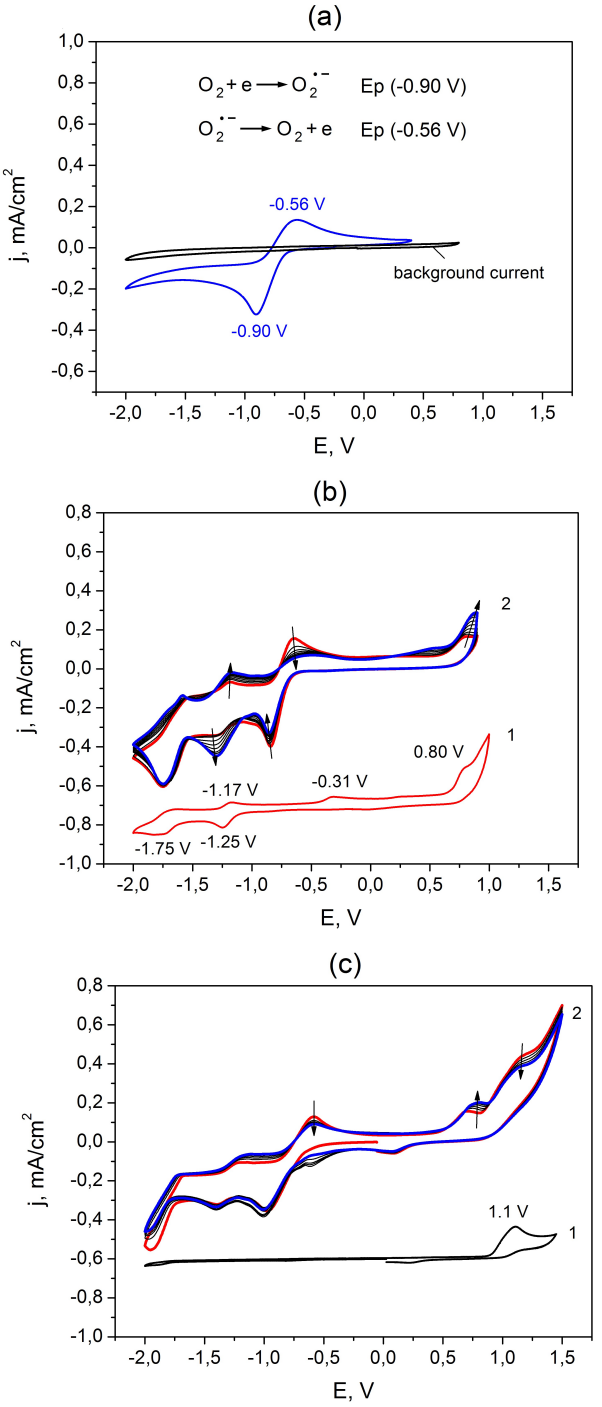

Figure 7. Electrochemical responses of DMSO solutions: (a) oxygenated; (b) Porph in degassed solution (1); ten consecutive cycles of Porph in oxygenated solution (2); (c) aniline in degassed solution (1); ten consecutive cycles of composite in oxygenated solution (2). The potential scan rate is 0.02 V/s.

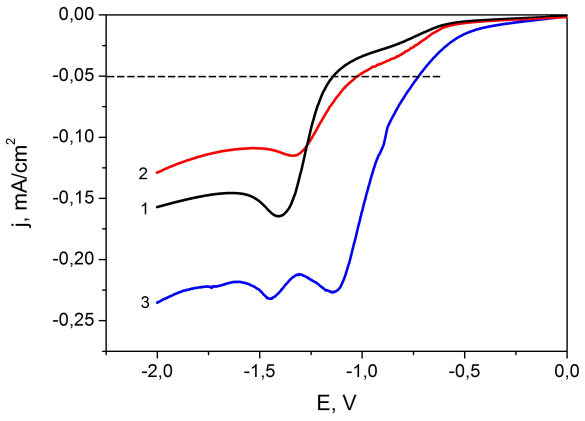

Figure 8. LSV of carbon dioxide electroreduction on: glassy carbon (1), polyporphyrin (2), composite material (3). The sweep rate of the potential is 0.01 V/s.

Conducting the carbon dioxide electroreduction process at the potential of one of the stages suggests the possibility of obtaining an individual product with a higher yield when using composite as a CO_2ERR catalyst.

Conclusion

In this work for the first time the possibility of forming composite film materials from mixtures of Porph and aniline components by electrodeposition when the process is initiated by superoxide anion radical. The addition of aniline changes the morphology and functional characteristics of the obtained material. Testing of Porph-based materials with aniline addition in the electrochemical carbon dioxide reduction reaction showed a shift of the onset of the process on the composite surface to the positive region compared to the onset of the process on glassy carbon and poly-Porph. We believe that this is due to the increased density of surface defects for composite film. Thus, composite formation can be a rather promising way to develop functional materials with improved properties.

Acknowledgements. The authors thank the Upper Volga Region Centre of Physico-Chemical Research (G.A. Krestov Institute of Solution Chemistry of the Russian Academy of Sciences) for technical support. The work was financially supported by the Ministry of Education and Science of the Russian Federation (Government Assignment No 122040500043-7).

Author Contribution. Svetlana A. Chulovskaya: Investigation, visualization, writing - original draft; Sergey M. Kuzmin: Conceptualization, methodology, investigation, writing - review and editing; Vladimir I. Parfenyuk: Supervision, writing - review and editing.

References

1. Park J.M., Lee J.H., Jang W.D. *Coord. Chem. Rev.* **2020**, *407*, 213157. https://doi.org/10.1016/j.ccr.2019.213157.
2. Cook L.P., Brewer G., Wong-Ng W. *Crystals* **2017**, *7*, 223. https://doi.org/10.3390/cryst7070223.
3. Li X., Lei H., Xie L., Wang N., Zhang W., *Cao R. Acc. Chem. Res.* **2022**, *55*, 878–892. https://doi.org/10.1021/acs.accounts.1c00753.
4. Bazanov M.I., Berezina N.M., Kokorin M.S., Semeikin A.S., Petrova D.V. *ChemChemTech. [Izv. Vyssh. Uchebn. Zaved. Khim. Khim. Tekhnol.]* **2023**, *66,* 46–55. https://doi.org/10.6060/ivkkt.20236609.6853.
5. Berezina N.M., Bazanov M.I., Berezina G.R., Lubimova T.V., Semeikin A.S. *ChemChemTech [Izv. Vyssh. Uchebn. Zaved. Khim. Khim. Tekhnol.]* **2024**, *68*(2), 62–69. https://doi.org/10.6060/ivkkt.20256802.7129.
6. Vu T.T., Luong T.D., Nguyen D.C., Le Vu.T., Bui T.T.T., Tran D.D., Hoang T.H., Vu D.M., Berezin D.B. *ChemChemTech [Izv. Vyssh. Uchebn. Zaved. Khim. Khim. Tekhnol.]* **2024**, *68*(2), 6–45. https://doi.org/10.6060/ivkkt.20256802.7002
7. Shorokhova T.V., Plotnikova A.O., Ivanova Yu.B., Lyubimova T.V., Lyubimtsev A.V., Kruk N.N., Syrbu S.A. *ChemChemTech [Izv. Vyssh. Uchebn. Zaved. Khim. Khim. Tekhnol.]* **2023,** *66*(12), 65–75. https://doi.org/10.6060/ivkkt.20236612.6819.
8. Day N.U, Wamser C.C, Walter M.G. *Polymer Int*. **2015**, *64*, 833-857. https://doi.org/10.1002/pi.4908.
9. Ji W., Wang T.X., Ding X., Lei S., Han B.H. *Coord. Chem. Rev*. **2021**, *439*, 213875. https://doi.org/10.1016/j.ccr.2021.213875.
10. Drouet S., Ballut S., Rault-Berthelot J., Turban P., Paul-Roth C. *Thin Solid Films* **2009**, *517*, 5474–5481. https://doi.org/10.1016/j.tsf.2009.01.107.
11. Bushuyev O.S., De Luna P., Dinh C.T., Tao L., Saur G., van de L. Jao., Kelley S.O., Sargent E.H. *Joule* **2018**, *2*, 825–832. https://doi.org/10.1016/j.joule.2017.09.003.
12. Kortlever R., Shen J., Schouten K.J.P., Calle-Vallejo F., Koper M.T.M. *J. Phys. Chem. Lett.* **2015**, *6*, 4073–4082. https://doi.org/10.1021/acs.jpclett.5b01559.
13. Kumar B., Brian J.P., Atla V., Kumari S., Bertram K.A., White R.T., Spurgeon J.M. *Catal. Today* **2016**, *270*, 19–30. https://doi.org/10.1016/j.cattod.2016.02.006.
14. Mukherjee A., Abdinejad M., Mahapatra S.S., Ruidas B.C. *J. Mater. Chem. A* **2023**, *11*, 9300–9332. https://doi.org/10.1039/D2TA08209H.
15. Abdinejad M., Motlagh M.K., Noroozifar M., Kraatz H.B. *Mater. Adv.* **2022**, *3*, 1224–1230. https://doi.org/10.1039/D1MA01057C.
16. Li Z., Wei Q., Ren Z., Xie J. *Molecules* **2025**, *30*, 2287. https://doi.org/10.3390/molecules30112287.
17. Dedi D., Dorniak A., Rinner U., Schöfberger W. *Front. Chem.* **2021,** *9*, 685619. https://doi.org/10.3389/fchem.2021.685619.
18. Yu P., Lv X., Wang Q., Huang H., Weng W., Peng C., Zhang L., Zheng G. *Small* **2023**, *19*, 2205730. https://doi.org/10.1002/smll.202205730.
19. Li J., Hou Y., Cui C.-X., Zhang X., Wang J.-C., Wang A., Chen Z., Li M., Lou T. *Dalton Trans*. **2022**, *51*, 15022-15030. https://doi.org/10.1039/D2DT02500K.
20. Weng Z., Jiang J., Wu Y., Wu Z., Guo X., Materna K.L., Liu W., Batista V.S., Brudvig G.W., Wang H. *Am. Chem. Soc.* **2016**, *138*, 8076–8079. https://doi.org/10.1021/jacs.6b04746.
21. Jiang H., Zhao P., Shen H., Yang S., Gao R., Guo Y., Cao Y., Zhang Q., Zhang H. *Small*, **2024,** *20,* 2304998. https://doi.org/10.1002/smll.202304998.

22. Kosugi K., Kashima H., Kondo M., Masaoka S. *Chem. Commun.* **2022**, ***58***, 2975–2978 https://doi.org/10.1039/D1CC0 5880K.
23. Esfandiari A., Abdinejad M., Seifitokaldani A. *J. Mater. Chem. A* **2025**, *13*, 19944. https://doi.org/10.1039/D5TA01319D.
24. Kuzmin S.M., Chulovskaya S.A., Parfenyuk V.I. *Electrochim. Acta* **2022**, *425*, 140742. https://doi.org/10.1016/j.electacta.2022.140742.
25. Parfenyuk V.I., Kuzmin S.M., Chulovskaya S.A., Filimonova Y.A. *Macroheterocycles* **2024**, *17*, 197–204. https://doi.org/10.6060/mhc245927p.
26. Kuzmin S.M., Chulovskaya S.A., Parfenyuk V.I. *J. Electroanal. Chem*. **2023**, *943*, 117594. https://doi.org/10.1016/ j.jelechem.2023.117594.
27. Chulovskaya S.A., Kuzmin S.M., Parfenyuk V.I. *Thin Solid Films* **2022**, *752*, 139245. https://doi.org/10.1016/j.tsf.2022.139245.
28. Balu K., Kaliyamoorthy S., Durai M., Aguiar A., Sobral M.C.M., Muthuvel I., Kumaravel S., Avula B., Sobral A.J.F.N., Ahn Y.-H. *Inorg. Chem. Commun*. **2023**, *154*, 110973. https://doi.org/10.1016/j.inoche.2023.110973.
29. Demel J., Lang K. *Eur. J. Inorg. Chem*. **2012**, 5154–516. https://doi.org/10.1002/ejic.201200400.
30. Garg K., Shanmugam R., Ramamurthy P.C. *Carbon* **2017**, *122*, 307-318. https://doi.org/10.1016/j.carbon.2017.06.052.
31. Kuzmin S.M., Chulovskaya S.A., Filimonova Y.A., Parfenyuk V.I. *J. Electroanal. Chem*. **2023**, *947*, 117798. https://doi.org/10.1016/j.jelechem.2023.117798.
32. Zhang Y., Jiang H., Wang K., Niu D., Zhang X. *J. Mater. Chem. A* **2023**, *11*, 20796–20807. https://doi.org/10.1039/D3TA04368A.
33. Wu J., Shi Q., Mu S. *Synth. Met*. **2019**, *255*, 116109. https://doi.org/10.1016/j.synthmet.2019.116109.
34. Kuzmin S.M., Chulovskaya S.A., Parfenyuk V.I. *Electrochim. Acta* **2025**, *535*, 146610. https://doi.org/10.1016/j.electacta.2025.146610.
35. Hayvalı M., Gündüz H., Gündüz N., Kılıç Z. ¸ Hökelek T. *J. Mol. Struct*. **2000**, *525*, 215–226. https://doi.org/10.1016/S0022-2860(00)00417-8.
36. Longo F.R., Finarelli M.G., Kim J.B. *Heterocycl. Chem*. **1969**, *6*, 927-931. https://doi.org/10.1002/jhet.5570060625.
37. Kuzmin S.M., Chulovskaya S.A., Parfenyuk V.I. *Mat. Chem. Phys*. **2020**, *241*, 122394. https://doi.org/10.1016/j.matchemphys.2019.122394.
38. Kuzmin S.M., Chulovskaya S.A., Parfenyuk V.I. *Electrochim. Acta* **2018**, *292*, 256–267. https://doi.org/10.1016/j.electacta.2018.09.127.
39. Parfenyuk V.I., Kuzmin S.M., Chulovskaya S.A., Koifman O.I. *Russ. Chem. Bull.* **2022**, *71*, 1921–1929.
40. Walter M.G., Wamser C.C., *J. Phys. Chem. C* **2010**, *114*, 7563. https://doi.org/10.1021/jp910016h.
41. El Aggadi S., Loudiyi N., Chadil A., El Zoubida A., El Hourch A. *Mediterranean J. Chem.* **2020**, *10*, 138–145. https://doi.org/10.13171/mjc102020021114sea.
42. Cai Y., Hu B., Wang X. *Front. Chem. Sci. Eng*. **2024**, *18*, 74. https://doi.org/10.1007/s11705-024-2427-z.
43. Xie C., Yan D., Li H., Du S., Chen W., Wang Y., Zou Y., Chen R., Wang S. *ACS Catal*. **2020**, *10*, 11082–11098. https://doi.org/10.1021/acscatal.0c03034.
44. Zhou Y., Chen S., Xi S., Han Y., Pang Y., Xia B.Y. *Cell Reports Phys. Sci*. **2020**, *1*, 100182. https://doi.org/10.1016/j.xcrp.2020.100182.
45. Nan J., Zhang L., Cao R., Zhu L., Chen G., Yan Q. *J. Org. Chem*. **2025**, *90*, 4277–4290. https://doi.org/10.1021/acs.joc.4c03189.
46. Sawyer D.T., Roberts J.L. *J. Electroanal. Chem*. **1966**, *12*, 90–101. https://doi.org/10.1016/0022-0728(66)80021-9.
47. Hoshi N., Murakami T., Tomita Y., Hori Y. *Electrochem*. **1999**, *67*, 1144–1146. https://doi.org/10.5796/ electrochemistry.67.1144.

Received 30.12.2025
Accepted 11.02.2026